Chem. Res. Chinese Universities, 2020, 36(4), 597—610 doi: 10.1007/s40242-020-0183-2

Review

Two-dimensional Noble Metal Nanomaterials for Electrocatalysis

SUN Rongbo, GUO Wenxin, HAN Xiao and HONG Xun*

Center of Advanced Nanocatalysis(CAN), Department of Applied Chemistry, Hefei National Laboratory for Physical Sciences at the Microscale, University of Science and Technology of China, Hefei 230026, P. R. China

Abstract Two-dimensional noble metal nanomaterials(2D NMNs) are widely used as electrocatalyst. In recent years, the researchers have focused on the synthesis of 2D NMNs at the atomic scale, and realize the improvement of electrocatalytic performance through further structural modification to reduce the usage of noble metals. Herein, we systematically introduce the synthesis methods of 2D NMNs categorized by element type. Subsequently, the catalytic applications toward a variety of electrocatalytic reactions are described in detail including the hydrogen evolution reaction(HER), oxygen reduction reaction(ORR), oxygen evolution reaction(OER) and CO_2 reduction reaction (CO_2RR). Finally, the potential opportunities and remaining challenges in this emerging research area are proposed.

Keywords Two-dimensional nanomaterial; Noble metal; Electrocatalysis

1 Introduction

Two-dimensional(2D) nanomaterials refer to materials with a size limit of nanoscale in one dimension and infinitely expandable in the other two dimensions[1,2]. By virtue of confined dimensionality, high specific surface areas, distinct geometric and electronic structure, and other fascinating physical and chemical properties, 2D nanomaterials have displayed prospective applications in various fields including catalysis, photonics, sensors, and storage devices[3—7]. Since the successful preparation of graphene through the mechanical exfoliation method in 2004, a new and exciting research frontier of 2D nanomaterials was opened up and gained rapid development[8,9]. So far, various 2D nanomaterials with size and shape control have been synthesized, such as transition metal dichalcogenides(TMDs), layered double metal hydroxides(LDHs), nitrides and carbonitrides(MXenes), etc.[10—15]. Thereinto, 2D noble metal nanomaterials(2D NMNs) give rise to unique reactivity patterns and have attracted extensive research interest in catalytic and energy applications due to their unique surface chemistry property and high specific surface area[16—19].

Electrocatalysis is a core technology of next-generation clean energy systems, such as fuel cells, electrolyzed hydrogen production, and metal-air batteries, which plays a key role in sustainable energy development[20—23]. The electrochemical reactions include hydrogen evolution reaction(HER), hydrogen oxidation reaction(HOR), oxygen evolution reaction(OER), oxygen reduction reaction(ORR) and CO_2 reduction reaction (CO_2RR), etc[24—28]. The noble metal-based catalysts are at the most defined core position of a wide variety of electrocatalytic materials[29—34]. Although many non-noble even non-metallic catalysts have been applied for electrocatalysis, their catalytic activity and stability still could not compare to those of noble metal catalysts[35—38]. It is worth noting that noble metal electrocatalysts are usually hindered by high prices and extremely limited reserves[39]. To solve the above problems, researchers have prepared high-performance electrocatalysts by regulating the morphology, structure and composition of noble metal materials, while reducing the usage of noble metals and the cost of energy systems[40,41]. 2D NMNs have become highly promising catalysts in the field of electrocatalysis because of their excellent intrinsic activity and highly exposed active sites[4,41]. For instance, Huang *et al.*[42] reported an electrochemical method to prepare a highly distorted porous 2D Pt nanosheet by electrochemical etching, and the optimized sample displays superior ORR performance. Their specific activity and ORR mass are 10.7 and 9.8 times that of commercial Pt/C catalysts. The large lateral size of the 2D NMNs makes it have a higher specific surface area, which is beneficial to expose larger amounts of active sites in the catalytic reaction and maximize the utilization of precious metals[43,44].

The demands for high-performance electrocatalyst have extremely stimulated the synthetic methods for preparing 2D NMNs[45]. Because the atoms in the metallic crystalline domain are closely located and firmly bonded together, there are certain limitations in the preparation of 2D NMNs by the exfoliation method compared to layered materials[46—48]. Therefore, most strategies for synthesizing 2D NMNs rely on the bottom-up wet-chemistry methods. Specifically, isotropic nuclei are generally formed early in the synthesis process, and then the anisotropic growth of the crystal is triggered by breaking its symmetry to drive the synthesis of ultra-small nuclei into 2D

*Corresponding author. Email: hongxun@ustc.edu.cn

Received June 14, 2020; accepted June 30, 2020.

Supported by the National Key R&D Program of China(Nos.2017YFA0700104, 2018YFA0702001), the National Natural Science Foundation of China(No.21871238) and the Youth Innovation Promotion Association of the Chinese Academy of Sciences(No.2018494).

morphologies[46,49]. Some generally adopted formation mechanisms include organic ligand-assisted growth, small molecules/ions mediated assisted growth, template synthesis and kinetic control, etc[50—52]. It is worth noting that these factors can synergistically affect the 2D morphology in the complicated growth system of 2D NMNs and achieve the delicate control of the product.

This review aims to comprehensively introduce the research progress made so far in the synthesis and application of various 2D and quasi-2D NMNs. First, we introduced the synthetic strategies of 2D NMNs categorized by element type, and demonstrate the mechanism of improving electrocatalytic performance through further structural modification. Next, the research progress of new 2D NMNs in the field of electrocatalysis(HER, OER, ORR, CO_2RR) was analyzed and summarized. Finally, on the basis of the current development, we pointed out the potential opportunities and remaining challenges for future research of 2D noble metal electrocatalysts.

2 Preparation of Two-dimensional Noble Metal Nanomaterials

Metal crystals usually exhibit highly symmetrical crystal structure(such as cubic crystal system), and the dominant metal bond is generally considered to be nondirectional[46,47,53,54]. Therefore, from the perspective of crystallography, it is difficult for metal crystals to spontaneously grow to obtain a 2D crystal structure with low symmetry. Meanwhile, the large surface energy of the exposed metal surface also blocks the acquisition of the metal 2D structure from the view of thermodynamics[55,56]. Hence, the anisotropic growth of materials can be realized accessibly by breaking and reducing the symmetry of metal crystal structure by introducing defects or adsorbates[57].

Despite these objective difficulties, a series of 2D NMNs was prepared. Synthetic methods that have been proposed include organic ligand assisted growth, small molecules/ions mediated assisted growth, photochemical synthesis, crystal phase transformation, template synthesis, kinetic control and exfoliation method, etc. In the following sections, typical examples of 2D NMNs composed of different elements will be categorized, and their unique characteristics will be emphasized.

2.1 Pt

In the field of electrocatalysis, Pt is an irreplaceable key material because of its high stability and high activity[39]. It is necessary to synthesize 2D Pt and Pt-based alloy structures with both high atomic utilization and rich catalytic activity sites, considering the rarity and high cost of Pt.

Matsumoto's research group[58] prepared 2D monolayer Pt nanosheets by the liquid stripping method. The layered Pt nanosheet precursors were primarily formed in the presence of K_2PtCl_4, hexamethylenetetramine(HMT) and sodium dodecyl sulfate(SDS). Then exfoliation and chemical/electrochemical reduction were performed to obtain 2D monolayer Pt nanosheets[Fig.1(A)]. Liu's research group[59] prepared 2D ultrathin single-crystal Pt nanodendrites (PtNDs) in aqueous solution[Fig.1(B)]. In this strategy, the properly designed C_{22}N-COOH(Br^-) amphiphilic surfactant acts as a template to guide the controlled synthesis of the 2D structure. The surface epitaxial growth of Pt nanocrystals was dynamically transformed into ultrathin PtND along the selectively exposed {111} facet.

Besides, the template method is also commonly used in the synthesis of 2D Pt nanomaterials. For example, Zhang and co-workers[60] used 2D nitrogen-doped graphene aerogels as templates to produce {111} surface-exposed Pt nanosheets by liquid-phase reduction. In the construction of 2D noble metal nanostructures, other 2D materials have also been extensively studied as templates. Gao and his colleagues[61] introduced the epitaxial growth of Pt on Ag nanoplates and further obtained 2D frusto-triangular Pt nanoplates surrounded by (111) plane after etching the Ag nanoplates[Fig.1(C)]. Remarkably, ORR performance test results showed that compared with the commercial Pt/C catalyst, the resulting ultrathin Pt nanoplates with the thickness of 1—2 nm increased the activity and the mass activity by 22 and 9.5 times, respectively. Gautam and co-workers[62] prepared 2D self-supporting Pt nanosheets by the mechanochemical transformation of the tellurium template. Zhang *et al.*[63] used monolayer MoS_2 as the reaction template and to obtain Pt-MoS_2 mixed nanosheet by liquid phase epitaxy growth.

Other transition metals also can be introduced to optimize the electronic structure and adsorption performance of the material[64,65]. Huang *et al.*[66] synthesized PtPb@Pt hexagonal nanosheet[Fig.1(D)—(F)] with Pt{110} exposed crystal surface, which has stable and efficient ORR performance. During the synthesis, PtPb intermetallic compounds nanosheets derived from the hexagonal crystal system were preferentially formed. And the remaining Pt precursors were reduced and deposited on the surface of the PtPb nanosheets, which continued to exist as *fcc* crystal structures. High angle annular dark field image scanning transmission electron microscope(HAADF-STEM) images showed that the nanoplate consisted of PtPb intermetallic compound nucleus and ultrathin Pt shell contained only four to six atomic layers. Similarly, Hou *et al.*[67] synthesized the triangular PtBi intermetallic compound nanosheets with the 2D structure in the oleamine system. By tuning the heating time, the lateral size of PtBi nanoplatelets(NPLs) can be easily controlled from 20 nm to 80 nm. As an excellent anode catalyst for formic acid or methanol oxidation, PtBi NPLs possess excellent resistance to CO poisoning. Moreover, Wang's group[68] proposed a gel-constrained nucleation/growth method to obtain PtCu nanosheets[Fig.1(G)—(I)]. The gel-like materials were first obtained during the synthesis process, and then the 2D nanostructure could be constructed by a straightforward heat-treatment process. The as-prepared PtCu nanosheets are 4—6 atom thickness with tunable lateral size from 10 nm to 50 nm and exhibit excellent electrocatalytic activity towards ethanol oxidation. On this basis, Zhang and co-workers[69] used PtCu nanoplates as templates to form PtCu@Pd core-shell nanoplates and reported the phenomenon of selective element diffusion[Fig.1(J)—(L)].

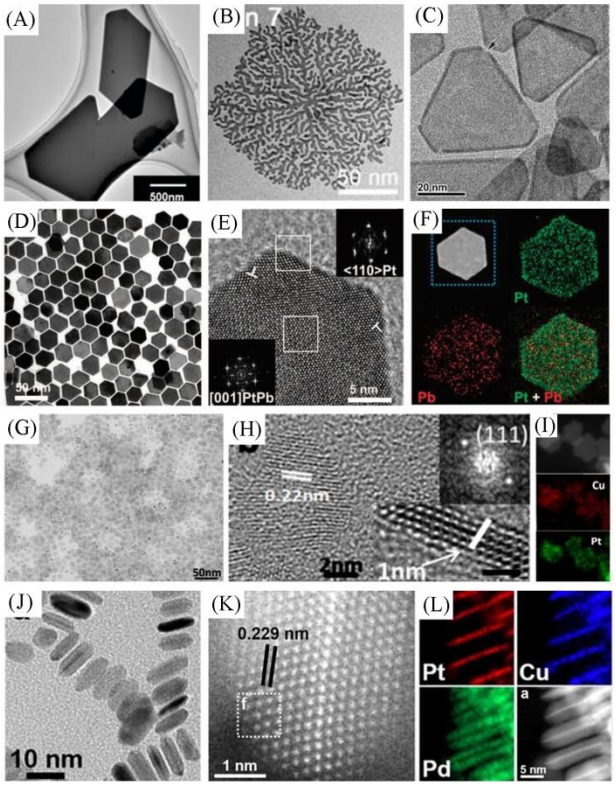

Fig.1 Characterization of 2D Pt and Pt-based nanomaterials

(A) TEM images of monolayer Pt nanosheets; reproduced with permission from ref.[58], Copyright 2014, Royal Society of Chemistry; (B) TEM images of 2D inorganic Pt nanodendrites; reproduced with permission from ref.[59], Copyright 2019, American Chemical Society; (C) TEM image of the ultrathin Pt nanoplates, the arrow indicates a defect; reproduced with permission from ref.[61], Copyright 2017, Royal Society of Chemistry; (D) TEM image of PtPb hexagonal nanoplates; (E) HRTEM of one single PtPb hexagonal nanoplate; inset: the FFT patterns from the white squares at the edge of and inside the nanoplate, respectively; (F) STEM EELS elemental mapping of PtPb hexagonal nanoplates; reproduced with permission from ref.[66], Copyright 2016, American Association for the Advancement of Science; (G) TEM image of PtCu nanosheets; (H) HRTEM image of PtCu nanosheets; inset: the corresponding FFT pattern; (I) HAADF image with corresponding spectral EDS elemental mapping; reproduced with permission from ref.[68], Copyright 2013, American Chemical Society; (J) TEM image of PtCu@Pd core-shell nanoplates; (K) aberration-corrected HAADF- STEM image of PtCu@Pd core-shell nanoplates; (L) HAADF-STEM and the corresponding EDS elemental mapping images; reproduced with permission from ref.[69], Copyright 2019, American Chemical Society.

2.2 Pd

Controllable synthesis of Pd-based nanocrystals by wet-chemical syntheses has been extensively reported, and Pd-based nanomaterials with varieties of shapes, for example, cubic, octahedral and 2D hexagonnanorods, can be produced[70,71]. Recently, Guo's research group[72] used a pot of wet-chemical method to synthesize ultrathin 2D PdMo nanosheets. The as-prepared 2D bimetallic nanosheets exhibit the sub-nanoscale thickness and highly curved state, which become the efficient catalysts for ORR and OER in alkaline electrolyte.

In addition to wet-chemical syntheses, the researchers have explored several synthetic methods for preparing 2D Pd nanomaterials. CO molecules preferentially form comparatively strong coordination bonds with the surface atoms of metal nanomaterials, thereby adsorbing on certain low refractive index surfaces of metals[73]. Therefore, an appropriate amount of CO can guide the anisotropic growth of 2D NMNs and is an effective shape regulator. The Remita's research group[74] synthesized ultrathin hexagonal Pd nanosheets by emulsion synthesis. The emulsion was produced by mixing the toluene solution of Pd precursors and the surfactant aqueous solution, and then CO was passed through the emulsion at low velocity for 15 min, thereby the ultrathin Pd nanoplates with the thickness of about 2 nm were gradually formed. The slow diffusion of CO leads to the retardatory nucleation of Pd and protects the surface of the crystal nucleus, which is crucial for regulating the 2D morphology of the nanosheets. Besides using an emulsion system, Zheng's group[75] reported a general CO-confined growth method to synthesize hexagonal Pd nanosheets. $Pd(acac)_2$ was reduced to Pd nanosheets in the aqueous system under a CO gas pressure of 1 bar(1 bar=10^5 Pa) [Fig.2(A)]. The as-prepared uniform Pd nanosheets exhibit controllable edge length with the range of 20—160 nm, and the thicknesses are less than 10 atomic layers. Furthermore, they demonstrated a facile synthesis of ultrathin 2D Pd nanosheets without any organic blocking agents(such as PVP) [Fig.2(B)][76]. The researchers processed H_2PdCl_4 in the CO atmosphere to prepare a Pd carbonyl complex, which was mixed with H_2O to realize the synthesis of ultrathin 2D Pd nanostructures.

In addition to obtaining uniform and independent 2D nanostructures, the stacked Pd nanosheet was also prepared through the addition of CO[Fig.2(C)][77]. The multilayer structure produces individual diffraction and Moiré patterns due to the thick layers of interconnected atoms stacked vertically and mismatched in rotation. The CO-limited growth method is not only applied to the preparation of pure 2D Pd nanostructures but also Pd-based alloy nanosheets. Han and co-workers[78] reported the production of 2D Pd-Pt-Ag ternary alloy nanostructures[Fig.2(D)—(F)]. In the aqueous solution with CO, the metal precursor was co-nucleated at a suitable molar ratio. The controlled synthesis of ultrathin 2D noble metal alloys opens a new opportunity to enhance the catalytic activity of noble metal nanostructures.

CO releasing agents(*e.g.*, carbonyl metal compounds) as the substitutes for CO are also commonly used in the synthesis of 2D NMNs[79]. These solid compounds will gradually decompose at high temperatures and release CO molecules. Recently, Zhang's group[80] have reported a straightforward way to synthesize controllable 2D PdCu alloy nanostructures [Fig.2(G)—(I)]. The ultrathin PdCu nanosheets were prepared by placing $Pd(acac)_2Cu(acac)_2$ and $Mo(CO)_6$ at 60 °C for 18 h in a mixture of trioctyl phosphine oxide and oleic acid.

Moreover, Xia *et al.*[81] obtained defective nuclei in the nucleation stage by the strategy of crystal growth kinetics control. It has been reported that by reducing the injection rate of Pd metal precursor in the reaction system, the kinetics control of crystal nucleation rate could be realized. Finally, Pd nanocrystals with different twin structures including 2D single

twin nanocrystals were obtained. Cheng *et al.*[82] prepared the 2D PdAg nanostructures by organic ligand assisted growth. The method of synthesizing 2D metal materials by using limb bundles as soft templates has high universality in composition. Tang *et al.*[83] reported a straightforward synthesis of 2D porous Pd nanosheets skillfully knitted by ultrathin nanowires. The self-assembly from low-dimensional nanomaterials has proven to be an effective method for synthesizing 2D NMN.

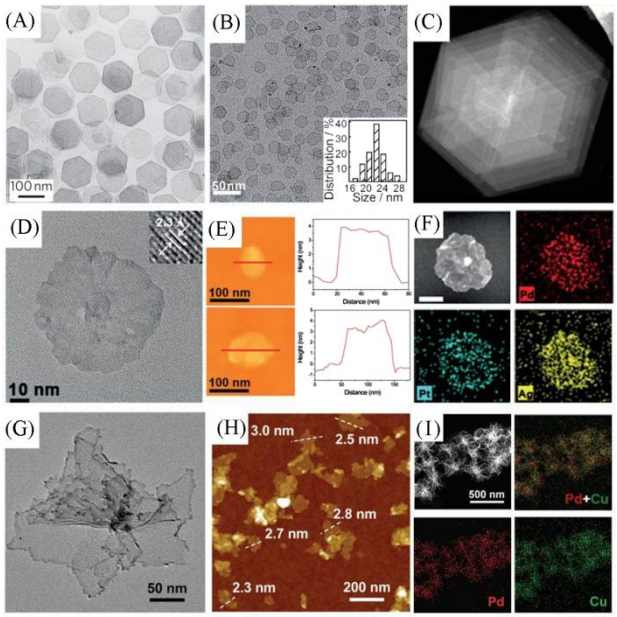

Fig.2 Characterization of 2D Pd and Pd-based nanomaterials

(A) TEM image of ultrathin Pd nanosheets synthesized in the presence of PVP and CTAB in DMF; reproduced with permission from ref.[75], Copyright 2011, Nature Publishing Group; (B) TEM image of the Pd nanosheets. Inset: the size distribution; reproduced with permission from ref.[76], Copyright 2013, WILEY-VCH; (C) ADF-STEM image of a multilayered Pd nanosheet at low magnification; reproduced with permission from ref.[77], Copyright 2014, American Chemical Society; (D) high-magnification TEM images of the Pd-PtAg nanosheets, inset: the visible lattice fringes; (E) AFM images and corresponding height profiles of Pd-Pt-Ag nanosheets supported on a Si wafer; (F) HAADF-STEM image and corresponding EDS elemental maps of a Pd-Pt-Ag nanosheet, scale bar is 20 nm; reproduced with permission from ref.[78], Copyright 2016, WILEY- VCH; (G) TEM image of the PdCu alloy nanosheets; (H) AFM image of the PdCu alloy nanosheets; (I) DF-STEM-EDS elemental mapping of the PdCu alloy nanosheets. Reproduced with permission from ref.[80], Copyright 2017, WILEY-VCH.

Graphene-based nanosheets represent one of the most important ultrathin 2D materials and offer a monolayer thickness characteristic that provides an ideal hard template for controllable metal 2D materials[50,84]. Yang *et al.*[85] used reduced graphene oxide(r-GO) as a template to prepare single crystal Pd square nanoplates surrounded by {100} crystal planes. Shen *et al.*[86] reported Pd-based PdM(M=Fe, Co, Ni) alloy nanoplates with exposed {111} crystal plane, which *in-situ* grows on the rGO by impregnation sintering method.

Particularly, the precise control of the 2D NMNs can greatly improve the material's atomic utilization efficiency, which can effectively enhance the catalytic activity and reducing the material loading and cost[87]. As shown in Fig.3(A) and (B), our group has reported a straightforward one-pot method for synthesizing Pd/Ru nanoribbons[88]. By ingeniously adding $RuCl_3 \cdot xH_2O$ solution, the ultrathin Pd nanosheets were broken to form atomically dispersed Ru on 2D Pd nanoribbons. The aberration corrected high-resolution transmission electron microscopy(HRTEM), synchrotron radiation photoemission spectroscopy(SRPES) and extended X-ray absorption fine structure (EXAFS) measurements proved that atomically dispersed Ru was successfully anchored on the surface of the 2D Pd nanoribbon, with Ru content up to 5.9%(mass fraction). Taking advantage of the synergistic effect between single-atom Ru and the ultrathin Pd substrate, this novel ultrathin Pd/Ru nanoribbons show superior catalytic performance for selective hydrogenation of C═C bonds, and remarkably prohibit the hydrogenolysis reaction. Compared with the commercial Pd/C and Ru/C, the Pd/Ru nanocatalysts exhibit excellent catalytic chemoselectivity. In addition, our group had also synthesized an ultrathin Pd nanomesh by a solution-based oxidative etching [Fig.3(C) and (D)][89]. By controlling the oxidation etching rate of ultrathin Pd nanosheets, the new type of 2D Pd nanomesh with uniform pore size distribution can be prepared. The as-prepared Pd nanomeshes possess an interconnected 2D network with densely arrayed, ultrathin quasi-nanoribbons and regular open holes. It's worth noting that the unique mesoporous structure makes these 2D Pd nanomeshes exhibit excellent catalytic property for ethanol electrooxidation. Besides, we have further utilized the regular mesh structure for supporting other noble metals, such as Pt, and the obtained Pt nanoparticles embedded in the ultrathin Pd NMs(Pd NMs/Pt) exhibit extremely high activity and durability towards HER.

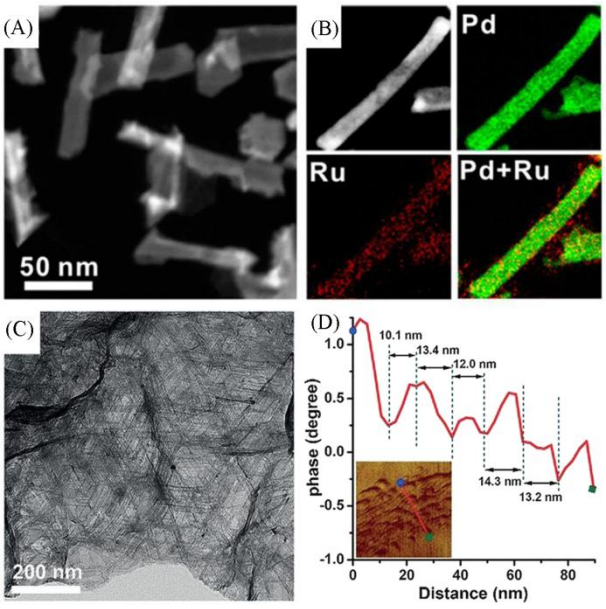

Fig.3 Precise control of the 2D Pd and Pd-based nanomaterials

(A) HAADF-STEM image of the Pd/Ru nanoribbons; (B) HAADF- STEM image of a Pd/Ru nanoribbon and the corresponding STEM-EDX elemental mapping; reproduced with permission from ref.[88], Copyright 2016, American Chemical Society; (C) TEM image of the ultrathin Pd nanomeshes; (D) AFM phase image(inset) and the corresponding width distribution of holes of the ultrathin Pd nanomeshes. Reproduced with permission from ref.[89], Copyright 2018, WILEY-VCH.

2.3 Au

The optical and catalytic properties of gold nanomaterials are very fascinating[12]. In recent years, various methods have been reported to synthesize 2D Au nanomaterials with controllable shape, size, crystal structure, and surface properties, which also provide fresh insights into the growth mechanism and catalytic performance of 2D materials[90—94].

The methods of synthesizing Au nanosheets are mainly divided into two categories: chemical synthesis and photocatalytic synthesis. In the chemical synthesis system, in addition to metal precursors, reducing agents and protective agents, the small molecules/ions can be added to promote the anisotropic growth of the product[95,96]. These ions mainly include halides (such as chloride, bromide and iodide), which possess a strong tendency to adsorb on the surfaces of metal. They can modulate the redox potentials of metal ions and act as a capping agent for specific crystal face, thereby guiding the growth of metal nanocrystals in specified directions[97—99]. For example, Zhang *et al.*[100] obtained high-quality monodispersed triangular Au nanoplates by oxidative etching of I_3^- ions. Furthermore, photocatalytic synthesis is another effective method to prepare 2D NMNs[101—104]. Wei *et al.*[105] reported a synthesis of 2D Au nanoprisms by plasmon-driven, and clarified the growth mechanism of photocatalytic synthesis at the level of single nanoparticles. The physical position of the surfactant polyvinylpyrrolidone(PVP) on a single Au nanostructure was detected at the molecular level using nanoscale secondary-ion mass spectrometry(NanoSIMS). The results show that PVP preferentially adsorbs at the boundary of the nanoprism rather than the top facet, thereby promoting the growth of 2D nanostructures.

Recently, 2D Au nanomaterials have also been synthesized by the template method. When using layered material as a template, the metal ions diffuse into the interlayer space primarily, and are then reduced *in-situ* by inserting a reductant or performing heat treatment therein. As shown in Fig.4(A) and (B), Jin's group[106] introduced extraordinary polymer-free iridescent lamellar hydrogels as a 2D soft template to guide the growth of 2D single-crystal Au nanosheets and successfully synthesized a free-standing and large-area single-crystal Au film with an atomic smooth surface. Ding and co-workers[107] used layered liquid crystal as a template to obtain Au nanosheets with a tunable thickness between 8 nm and 100 nm by photochemical synthesis shown in Fig.4(C). Moreover, Xiao *et al.*[108] made layered double hydroxides as templates and used anion exchange to reduce Au^{3+} ions diffusing between the layers through sodium borohydride to Au nanosheet. The as-prepared 2D Au nanostructures are single crystals with the thickness of several atomic layers and (001) basal plane [Fig.4(D)].

Zhang's group has made numerous achievements in the crystal phase modulation of 2D gold nanomaterials, such as the synthesis of stable *hcp*-Au nanosheets under normal temperature and pressure conditions[109]. As shown in Fig.5(A)—(C), for the first time, this group used graphene oxide(GO) as the template to synthesize the pure *hcp*-Au nanosheets. The

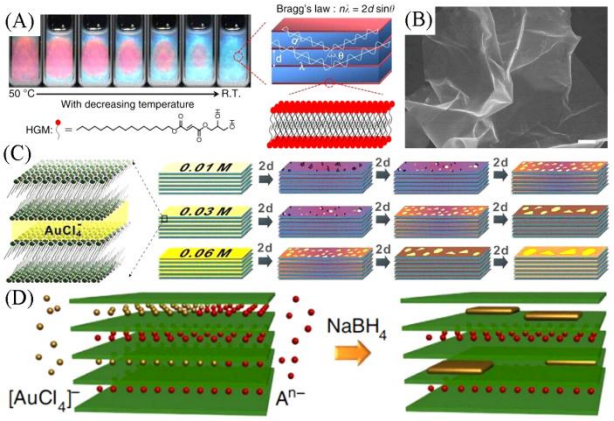

Fig.4 Schematic diagrams of three methods using layered materials as templates

(A) and (B) The synthesis template: polymer-free iridescent lamellar hydrogels, and the corresponding scanning electron microscopy of a typical Au membrane(scale bar, 1 mm). Reproduced with permission from ref.[106], Copyright 2014, Nature Publishing Group; (C) the synthesis template: layered liquid crystal; reproduced with permission from ref.[107], Copyright 2014, Royal Society of Chemistry; (D) the synthesis template: layered double hydroxides; reproduced with permission from ref.[108], Copyright 2015, Nature Publishing Group.

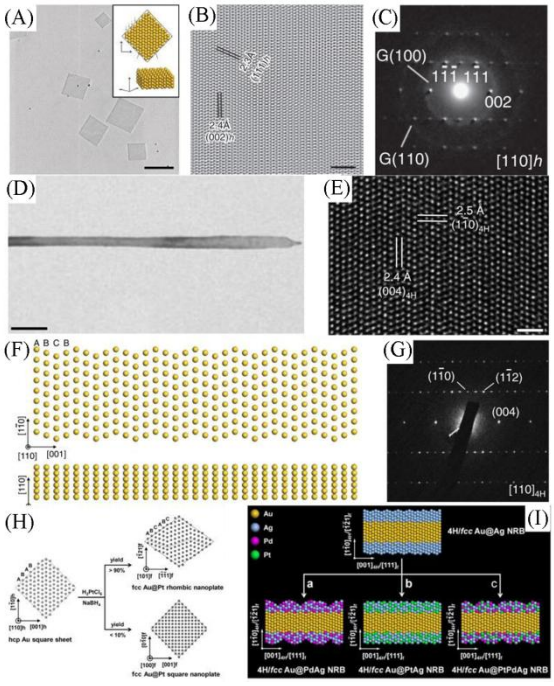

Fig.5 Crystal phase modulation of 2D Au nanomaterials

(A) TEM image, scale bar is 500 nm. Inset: crystallographic models for a typical *hcp*-Au nanosheets; (B) HRTEM image, scale bar is 2 nm; (C) SAED pattern; reproduced with permission from ref.[109], Copyright 2011, Nature Publishing Group; (D) TEM image of a typical Au NRB, scale bar is 100 nm; (E) aberration-corrected HRTEM image taken in the centre of an Au NRB, scale bar is 1 nm; (F) crystallographic models illustrating the top view (top panel) and side view(bottom panel) of a typical 4H Au NRB; (G) SAED pattern; reproduced with permission from ref.[110], Copyright 2015, Nature Publishing Group; (H) schematic illustration of the synthesis of *fcc*-Au@Pt rhombic nanoplates; reproduced with permission from ref.[111], Copyright 2015, Wiley-VCH; (I) schematic illustration of the 4H/*fcc*-Au@PdAg, Au@PtAg and Au@PtPdAg core-shell NRBs. Reproduced with permission from ref.[112], Copyright 2016, American Chemical Society.

thickness of these *hcp*-Au nanosheets is (2.4±0.7) nm(about 16 Au atomic layers), and the lateral size is 200—500 nm. The basic plane is the {100} plane, and the exposed four sides are the {112} planes. Under beam irradiation, the pure *hcp*-Au nanosheets can be changed into *fcc* structures. Besides the 2H phase, the team further synthesized another *hcp* phase of the gold nanostructure(4H phase) by the template-free wet-chemical method[Fig.5(D)—(G)][110]. On this basis, Zhang's research group[111] prepared ultrathin *fcc*-Au@Pt rhombic nanoplates by epitaxial growth of Pt on *hcp*-Au square nanosheets. The growth of the Pt layer induced the Au nanosheet as the substrate to undergo a phase transition from *hcp* to *fcc*[Fig.5(H)]. In addition, 4H-Au has been used as the growth template to direct the epitaxial growth of a range of metals and alloys adopting 4H phase, opened up a fresh strategy for the synthesis of anomalous 2D NMNs[Fig.5(I)][112,113].

2.4 Ag

It has been noted that Ag has many similar properties with Au, for example, high conductivity and high surface plasmon resonance(SPR) absorption in visible spectrum[114]. Nevertheless, the crystal nucleation and growth behavior of sensitive metals(*e.g.*, Au, Ag) are affected by the electromagnetic environment. In early studies, the formation of 2D Ag nanofilms is often induced by adjusting the wavelength of external light[115—117].

In addition to the method of synthesizing 2D Ag nanoplates by a photochemical reduction reaction, various strategies have been developed. Byun's group[118] prepared 2D Ag nanoplates with adjustable shape by small molecule and ion-assisted methods, in the process of which the influence of halogen ions on the formation of 2D Ag nanoplates had been systematically studied. The results show that halide ions can promote the vertical growth of crystal by selectively depositing Ag on the seeds of nanoplates, thus significantly affecting the 2D morphology.

The nucleation control can also be realized in the crystal growth kinetics by using the oxidizing group as the etchant, thereby obtaining the crystal nucleus with stacking faults or twins[100]. This method has also shown more extensive application in the synthesis of Ag nanosheets. For instance, Yin *et al.*[119] obtained high-quality triangular Ag nanosheets by the oxidation and etching of H_2O_2. In this method, all kinds of silver sources can be straightly converted into 2D morphology with appropriate end-capped ligands, which significantly improves the repeatability of synthesis. Similarly, Kawazumi and co-workers[95] have studied the rapid morphological transformation of crystal silver from sphere to prism in H_2O_2 aqueous solution. Xia *et al.*[120] demonstrated that the type of sealant present in the reaction solution would determine whether the growth pattern of Ag nanowires is horizontal or vertical.

Recently, Wu *et al.*[121] have prepared Ag nanosheets by the mechanical compression process. As shown in Fig.6(A), the first step in the preparation is to stack Ag(or Au, Fe, approximately 70 μm) foil with sacrificial foil, and then to fold and mechanically roll the foil 20 times, thereby the binary metal plates(about a few nanometers thick) can be obtained consisting of a large number of alternating layers of metal nanometers. The second step is to selectively etch the sacrificial metal to obtain the independent ultrathin 2D metal nanosheet. The average thickness of Ag nanosheets manufactured by this method is about 4 nm, and the average transverse size is about 3—5 μm[Fig.6(B)—(D)].

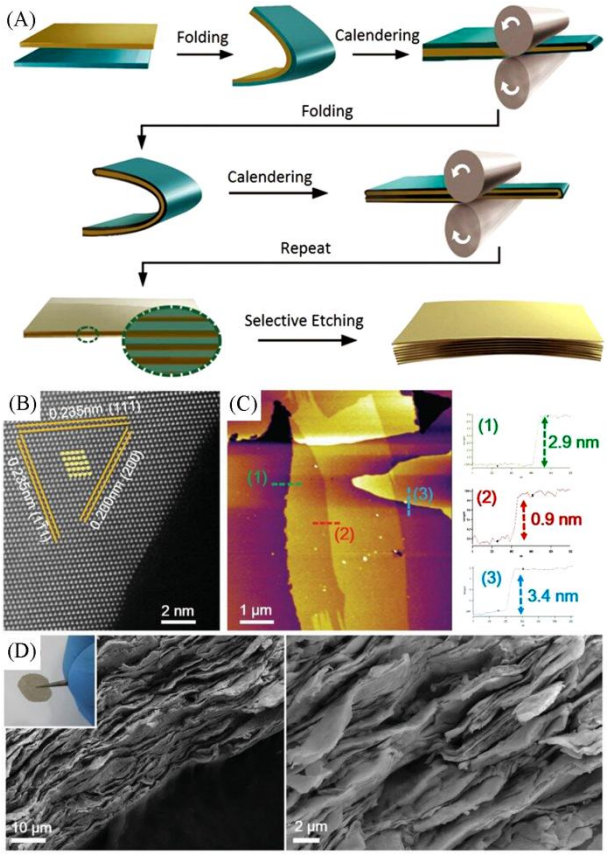

Fig.6 Mechanical compression process

(A) Schematic illustration of the fabrication of metal nanosheets to advance from thin metals toward their 2D nanolayer structures; (B) atomic-resolution annular bright-field(ABF) image of Ag nanosheet; (C) AFM image of three Ag-nanosheet layers with thickness of 2.9, 0.9, and 3.4 nm; (D) cross-sectional SEM images of the obtained Ag nanosheet film after suction filtration(left: low magnifications, right: high magnifications). Insets: photograph of a freestanding Ag nanosheets "paper" after suction filtration. Reproduced with permission from ref.[121], Copyright 2016, WILEY-VCH.

2.5 Rh

As a member of noble metal elements, Rh is one of the rarest metals, and also plays a significant role in electrocatalysis processes[122]. For the majority of reactions catalyzed by 2D nanomaterials, there is a strong correlation between selectivity/activity and surface atomic structure, which has led to a great deal of researches on the synthesis of 2D Rh nanocrystals[49].

Small molecule adsorbents are frequently used in the synthesis of 2D NMNs. The most typical example is CO, which can be selectively adsorbed on the specific crystal plane of some transition metal monomers or alloys. As shown in Fig.7(A) and (B), Zheng's group[123] has reported an efficient CO-assisted growth strategy for the preparation of single-crystal Rh nanosheets with atomic thickness and controllable

size. The detailed mechanism study shows that the formation process of Rh nanosheets is divided into two steps. In the early stage, small Rh carbonyl clusters with a size of 1—2 nm formed dispersedly. As the reaction proceeded, the Rh carbonyl clusters tended to aggregate together and shape into the typical 2D morphology to minimize the surface energy. It is discernable that the size of the nanosheets increased with the reaction time.

Besides, formaldehyde molecules also play a similar role in the preparation of 2D NMNs due to the strong selective adsorption of carbonyl groups on the metal. Using acetylacetone Rh as the precursor and formaldehyde as the shape controller, Zheng's group[124] synthesized 2D Rh nanofilms with the thickness of about 1 nm by simple hydrothermal method without surfactant. Li's *et al.*[125] synthesized semi-transparent ultrathin Rh nanosheets with an edge length of 500—600 nm through the solve-thermal method[Fig.7(C) and (D)]. The 2D NMNs synthesized by using small molecules/ion modifiers as soft templates generally possess high structural uniformity, and the exposed crystal plane of the obtained metal nanostructures is determined by the specific adsorbents used.

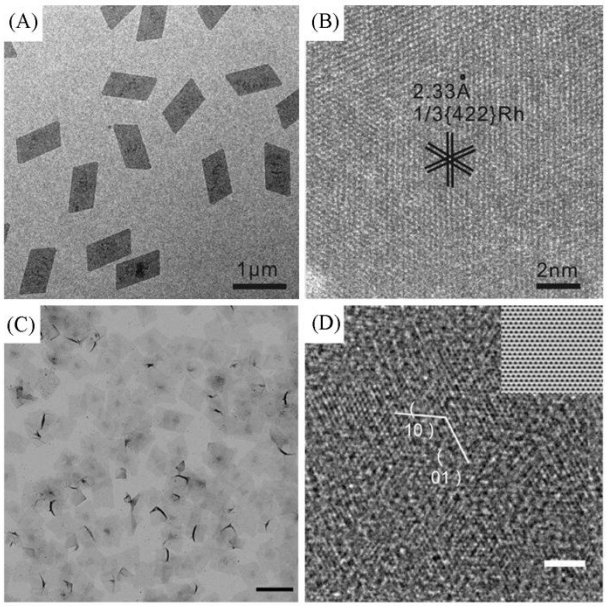

Fig.7 Characterization of 2D Rh nanomaterials

(A) TEM image of Rh nanosheets; (B) high-resolution HAADF-STEM image projected along the [111] axis of Rh nanosheets; reproduced with permission from ref.[123], Copyright 2015, WILEY-VCH; (C) low-magnification TEM image of the PVP-capped ultrathin Rh NSs; scale bar, 2 nm; (D) high-magnification TEM image of the PVP-capped Rh NSs. Scale bar, 100 nm. Reproduced with permission from ref.[125], Copyright 2014, Nature Publishing Group.

2.6 Ir and Ru

Ir has been widely used as a best-performing electrocatalyst for OER. Recently, a wet-chemical synthesis method of Ir-based superstructures composed of ultrathin nanosheets has been reported[Fig.8(A)][126]. In this synthesis, iridium chloride (III) can be reduced by benzyl alcohol in the presence of citric acid, glyoxal and poly(vinyl pyrrolidone). The obtained Ir superstructure was constructed by many 2D building blocks. This work promotes the further improvement of electrocatalytic performance by rationally combining 2D NMNs with 3D structures. Yamauchi's group[127] prepared 2D mesoporous metal Ir nanosheets through a simple wet-chemical reduction route, which is the first report to synthesize a 2D mesoporous metal nanosheet[Fig.8(B)]. Specifically, dissolve poly(ethylene oxide)-b-polystyrene(PEO-b-PS) in DMF, then mix with $IrCl_3$ aqueous solution and formic acid and keep the solution in a water bath at 80 °C for 5 h. In the reaction, PEO-b-PS micelle is a sacrificial pore guide agent to produce mesopores, and the degradation of formic acid produces CO to control the generation of 2D topography. This fresh 2D mesoporous metal nanostructure effectively increases the specific surface area of the material and makes the material receive abundant catalytic active sites.

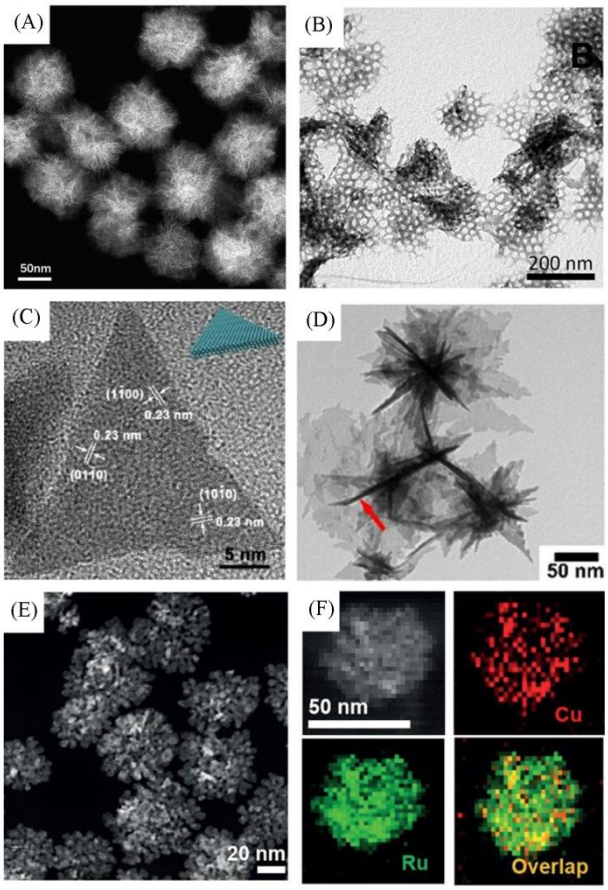

Fig.8 Characterization of 2D Ir, Ru and Ru-based nanomaterials

(A) HAADF-STEM image of 3D Ir superstructure; reproduced with permission from ref.[126], Copyright 2016, American Chemical Society; (B) TEM image of mesoporous Ir nanosheets; reproduced with permission from ref.[127], Copyright 2018, American Chemical Society; (C) HRTEM image of triangle Ru nanoplates; insets: the geometric model of the nanoplates; reproduced with permission from ref.[128], Copyright 2012, American Chemical Society; (D) TEM images of Ru nanosheets; reproduced with permission from ref.[129], Copyright 2016, American Chemical Society; (E) HAADF-STEM image of RuCu NSs; (F) HAADF-STEM-EDS elemental mappings of RuCu NSs; reproduced with permission from ref.[130], Copyright 2019, WILEY-VCH.

Unlike typical transition metals, Ru usually adopts the *hcp* crystal phase. Yan *et al.*[128] reported the preparation of triangular Ru nanofilms with adjustable edge length and

thickness by the hydrothermal method[Fig.8(C)]. DFT calculation demonstrates that the formation of the nanostructure is due to the selective adsorption of some small facet selectors and the inherent Ru crystal characteristics. Peng and his colleagues[129] reported an independent 2D Ru nanosheet with a significantly exposed low energy (001) surface[Fig.8(D)]. The formation of Ru nanosheet was initiated by the self-decomposition of Ru(III) metal precursor, thereby leading the growth of nanosheets, in which isopropanol and urea play a key role in determining the final 2D morphology.

Recently, some 2D alloy precious metal sheets have also been prepared. Huang's group[130] prepared a novel RuCu snowflake NS, which is composed of crystalline Ru and amorphous Cu and serves as a highly efficient electrocatalyst for OER and HER[Fig.8(E) and (F)]. Li *et al.*[131] reported a stable cobalt-substituted ruthenium nanosheet. The HAADF-STEM and XAFS results demonstrated that the cobalt atoms in the nanosheet are isolated in the ruthenium lattice. In alkaline HER reaction, its catalytic performance is better than those of commercial Pt/C catalyst and other Pt-free catalysts.

In addition, 2D amorphous Ir nanomaterials have been modulated and exhibited excellent OER performance. As shown in Fig.9, our group[132] proposed a general and effective route for preparing dozens of different amorphous noble metal nanosheets with thickness less than 10 nm by directly annealing the mixture of metal acetylacetonate and alkali salts. By precisely controlling annealing temperature and types of alkali salts, besides monometal NS, such as amorphous Ir NSs, amorphous Ru NSs and amorphous Rh NSs, dozens of different amorphous bimetal NSs and trimetal NSs can be successfully and conveniently prepared, such as RhFe NSs, IrRu NSs and IrRuRh NSs.

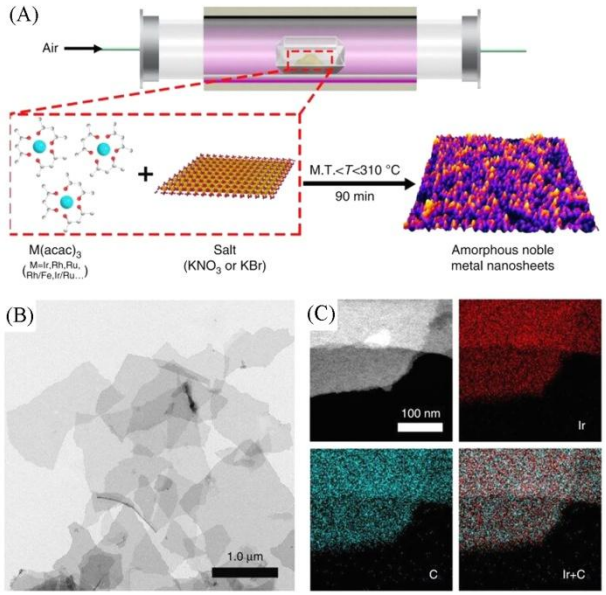

Fig.9 2D amorphous Ir nanomaterials

(A) Schematic illustration of the general synthetic process for amor- phous noble metal noble metal nanosheets(NSs); (B) TEM image of amorphous Ir NSs; (C) HAADF-STEM image and the corresponding EDS elemental mapping of amorphous Ir NSs. Reproduced with permission from ref.[132], Copyright 2019, Nature Publishing Group.

The schematic diagram of two-dimensional noble metal nanomaterials and the morphologies of these catalysts are displayed in Fig.10.

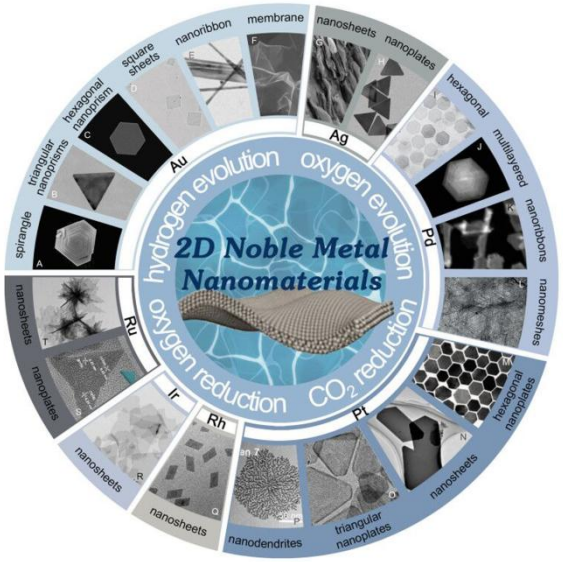

Fig.10 Schematic diagram of two-dimensional noble metal nanomaterials and morphologies of these catalysts displayed in the outer most circle

(A) Reproduced with permission from ref.[93], Copyright 2011, Royal Society of Chemistry; (B) reproduced with permission from ref.[104], Copyright 2012, American Chemical Society; (C) reproduced with permission from ref.[105], Copyright 2016, Nature Publishing Group; (D) reproduced with permission from ref.[109], Copyright 2011, Nature Publishing Group; (E) reproduced with permission from ref.[110], Copyright 2015, Nature Publishing Group; (F) reproduced with permission from ref.[106], Copyright 2014, Nature Publishing Group; (G) reproduced with permission from ref.[121], Copyright 2016, WILEY-VCH; (H) reproduced with permission from ref.[120], Copyright 2011, WILEY-VCH; (I) reproduced with permission from ref.[75], Copyright 2011, Nature Publishing Group; (J) reproduced with permission from ref.[77], Copyright 2014, American Chemical Society; (K) reproduced with permission from ref.[88], Copyright 2016, American Chemical Society; (L) reproduced with permission from ref.[89], Copyright 2018, WILEY-VCH; (M) reproduced with permission from ref.[66], Copyright 2016, American Association for the Advancement of Science; (N) reproduced with permission from ref.[58], Copyright 2014, Royal Society of Chemistry; (O) reproduced with permission from ref.[61], Copyright 2017, Royal Society of Chemistry; (P) reproduced with permission from ref.[59], Copyright 2019, American Chemical Society; (Q) reproduced with permission from ref.[123], Copyright 2015, WILEY-VCH; (R) reproduced with permission from ref.[132], Copyright 2019, Nature Publishing Group; (S) reproduced with permission from ref.[128], Copyright 2012, American Chemical Society; (T) reproduced with permission from ref.[129], Copyright 2016, American Chemical Society.

3 Application of 2D Noble Metal Materials in Electrocatalysis

In order to obtain low-cost and sustainable energy, a variety of 2D NMNs have been explored as photo- and electrocatalysts for energy-related reactions. HER, OER, ORR and CO_2RR are the core of clean energy conversion technology in the future[133—136]. The high-efficiency catalysts engineering for these catalytic reactions is of great significance for clean and sustainable development. The rich chemical and physical

properties of 2D NMNs provide opportunities for exploiting their applications in energy catalysis.

3.1 Hydrogen Evolution Reaction(HER)

Hydrogen is a clean and sustainable energy carrier with ultra-high energy density(about 140 kJ/g)[137]. It is considered as one of the most potential alternatives to fossil fuels. Among various hydrogen production technologies, electrolysis of water for hydrogen production(HER) has attracted much attention from researchers due to its clean characteristic and high purity of hydrogen produced[138,139].

In 2D noble metal electrocatalysts, Pt has been extensively studied due to its high inherent HER activity[140,141]. Zhang's group[63] prepared 2D Pt-MoS_2 hybrid nanostructures by epitaxial growth using 2D MoS_2 nanosheets as templates. The optimized Pt-MoS_2 hybrid nanostructure displays HER performance superior to the commercial Pt catalyst at the identical Pt loading. Besides, the 2D ultrathin single crystal Pt nanodendrites(PtNDs) synthesized by Liu *et al.*[59] exhibited excellent electrocatalytic HER performance. Meanwhile, a great number of studies have revealed atomically dispersed platinum catalyst with enhanced catalytic performance and stability. Wu's group[142] has presented a new structure with the submonolayer Pt controllably deposited on an intermetallic Pd_3Pb nanoplate(AL-Pt/Pd_3Pb), which exhibited an outstanding HER activity in acidic media. Our group[143] synthesized a unique Cu-Pt dual site alloyed Pd nanoring based on atomica modification on ultrathin Pd nanorings. XAFS confirmed the ultrafine structure comprising atomically dispersed Cu-Pt dual sites on the 2D nanorings, which is the active site for the catalytic reaction. This new trimetallic alloy catalyst exhibits excellent HER catalytic activity in acidic environment, with only 22.8 mV overpotential at a current density of 10 mA/cm^2, and has a high mass current density[Fig.11(A) and (B)]. This research group also developed a high-efficiency and stable HER catalyst with Pt nanoparticles dispersed on Pd nanomesh. (Pd NMs/Pt)[89]. Impressively, the overpotential of the Pd NMs/Pt at 10 mA/cm^2 is only 21.3 mV, which is the smallest one among all the electrocatalysts evaluated[Fig.11(C)]. And Fig.11(D) shows the long-term cycle stability of the Pd NMs/Pt.

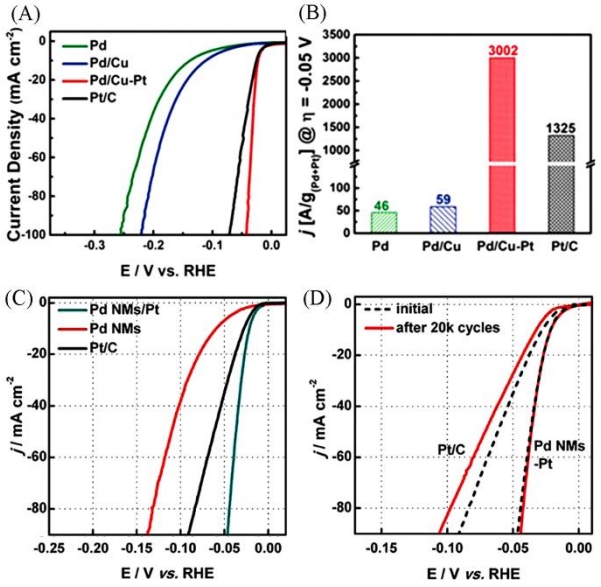

Fig.11 Electrochemical HER performances

(A) The HER polarization curves of Pd nanosheets, Pd/Cu nanorings, Pd/Cu-Pt nanorings and commercial Pt/C in 0.5 mol/L H_2SO_4 solution with a scan rate of 5 mV/s at room temperature; (B) HER mass activity normalized by mass of Pd and Pt at –0.05 V of the four catalysts; reproduced with permission from ref.[143], Copyright 2017, WILEY-VCH; (C) polarization curves of Pd NMs/Pt, Pd NMs and commercial Pt/C electrocatalysts in 0.5 mol/L H_2SO_4 solution with a scan rate of 5 mV/s; (D) durability test of Pd NMs/Pt and commercial Pt/C. Reproduced with permission from ref.[89], Copyright 2018, WILEY-VCH.

In addition, some of the 2D non-platinum catalysts also show prominent HER catalytic activity. Huang's group[130] reported a channel-rich RuCu snowflake nanosheet composed of crystalline Ru and amorphous Cu. The prepared RuCu NSs/C was annealed in air at 250 °C for 1 h(expressed as RuCu NSs/C-250 °C), and the HER activity was evaluated. The optimized sample displays superior performance under acidic and alkaline conditions due to the structural advantages. The 4H/*fcc*-Au@PdAg NRBs prepared by Zhang *et al.*[113] exhibit excellent activity when used as HER electrocatalysts, even comparable to the commercial Pt/C.

3.2 Oxygen Evolution Reaction(OER)

OER is a key reaction in sustainable energy systems, such as electrolyzed water and metal-air cells. Since OER is a four-electron transfer reaction, overcoming the kinetic barrier requires a higher energy than HER[144]. It is well known that Ir-based materials usually exhibit excellent catalytic properties in OER. In recent years, the controllable synthesis of 2D Ir and its application in OER have been widely reported[127,132].

Yamauchi *et al.*[127] reported a novel synthesis strategy to prepare 2D mesoporous metallic Ir nanosheets. Since the mesoporous structure increases the surface area of the material, the usability of the active site was improved. Compared with commercial catalysts and other Ir-based nanomaterial catalysts, 2D mesoporous metallic Ir nanosheets exhibit added OER catalytic activity under the acidic conditions. The overpotential of 2D mesoporous metallic Ir nanosheets is only 240 mV at the current density of 10 mA/cm^2 *vs.* RHE. In addition, it has a lower Tafel slope(49 mV/dec) in 0.5 mol/L H_2SO_4 electrolyte.

Impressively, as shown in Fig.12(A)—(C), the 2D amorphous Ir nanosheets prepared by our group[132] display excellent acidic OER performance. Compared with crystalline Ir nanosheets and commercial IrO_2 catalysts, the mass activities of the as-prepared sample were increased by 2.5 and 17.6 times, respectively. *In-situ* X-ray absorption fine structure spectroscopy shows that during the OER catalysis process, the valence state of Ir has increased(invariably less than +4 valence) and returned to the original state after the reaction[Fig.12(D) and (E)]. In addition, the atomic structure of the 2D amorphous Ir nanosheets remains stable and has excellent stability through the long-term durability test[Fig.12(F)]. These 2D

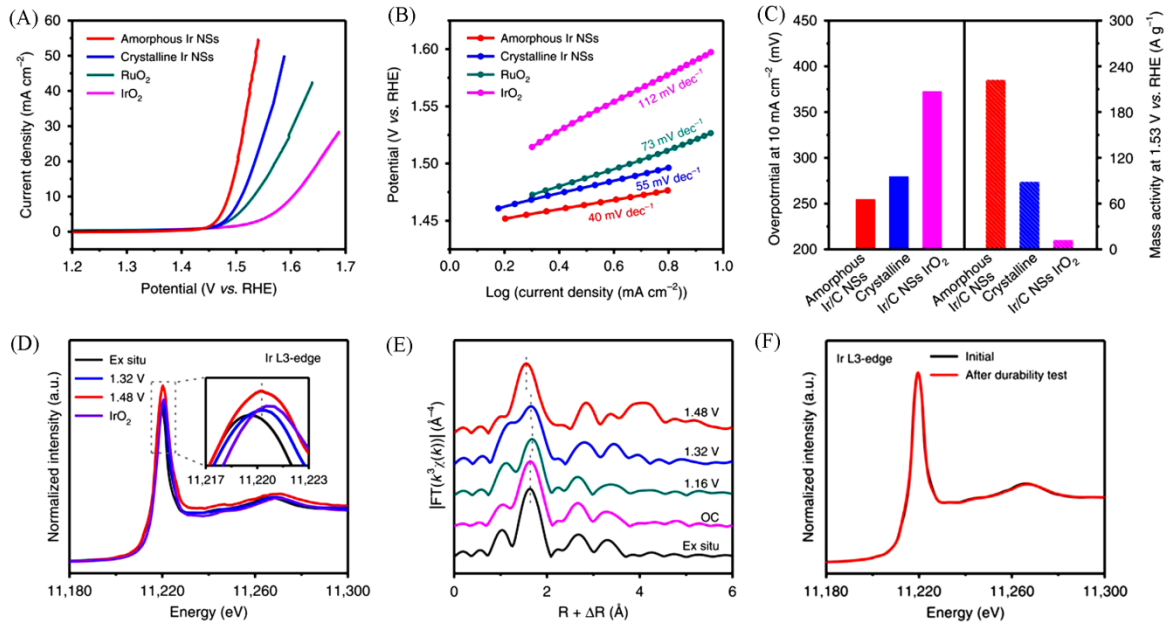

Fig.12 Electrochemical OER performance and operando X-ray absorption spectroscopy of amorphous Ir NSs

(A) Polarization curves of amorphous Ir NSs, crystalline Ir NSs, commercial RuO_2 and IrO_2 catalysts, respectively; (B) corresponding Tafel plots of amorphous Ir NSs, crystalline Ir NSs, commercial RuO_2 and IrO_2 catalysts, respectively; (C) overpotentials at 10 mA/cm^2(left axis) and mass activity at 1.53 V(*vs*. RHE)(right axis) of amorphous Ir NSs, crystalline Ir NSs, and commercial IrO_2 catalyst, respectively; (D) *in-situ* XAFS spectra change of the Ir L_3-edge; (E) *in-situ* XAFS spectra change of the Ir L_3-edge; (F) XANES spectrum of amorphous Ir NSs after durability test. Reproduced with permission from ref.[132], Copyright 2019, Nature Publishing Group.

amorphous Ir nanosheets are currently reported as one of the most remarkable OER electrocatalysts under acidic conditions.

3.3 Oxygen Reduction Reaction(ORR)

Polymer electrolyte membrane fuel cell(PEMFC) as an electrochemical power generation device with high power density, fast start-up speed, clean and high efficiency has a wide application prospect in electric vehicles, aerospace and other fields[145,146]. Among them, the cathodal ORR became the bottleneck for fuel cell development due to sluggish kinetics[147]. Although Pt suffers from the exorbitant price, it still plays an important role in the application and study of ORR catalysts.

Huang's group[66] synthesized PtPb@Pt hexagonal nanosheets with Pt{110} exposed crystal planes. Electrochemical tests showed that at 0.9 V, the specific activity and mass activity of PtPb@Pt nanosheets reached 7.8 mA/cm^2 and 4.3 A/mg, respectively[Fig.13(A) and (B)]. At the same time, the decay inactivity after 50000 voltage cycles is negligible, which indicates that they have excellent long-term durability. Recently, they also prepared a porous Pt nanosheet by electrochemical corrosion of ultrathin $PtTe_2$ NSs[42]. The specific surface area of the material was increased by introducing the porous structure, thereby greatly improving the utilization rate of surface active sites. The prepared E-Pt NSs showed enhanced ORR activity with mass activity(2.07 A/mg_{Pt}) and specific activity(3.1 mA/cm^2) at 0.90 V, which are 9.8 and 10.7 times that of the commercially available Pt, respectively [Fig.13(C) and (D)]. Besides, Matsumoto and co-workers[58] reported a 2D Pt nanosheet obtained by exfoliating layered platinum oxide, which showed enhanced ORR activity in alkaline electrolytes.

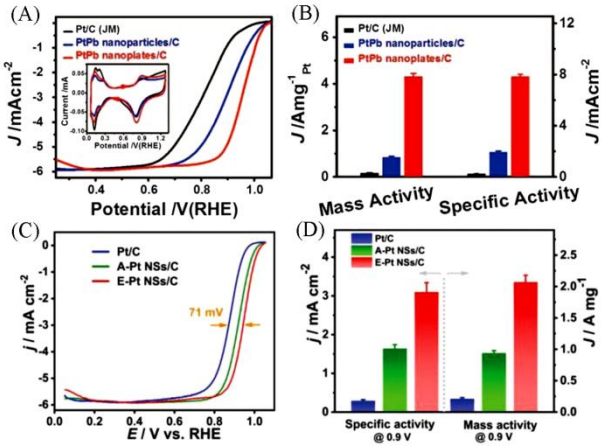

Fig.13 Electrochemical ORR performances

(A) ORR polarization curves of PtPb nanoplates/C, PtPb nanoparticles/C, and commercial Pt/C catalysts; (B) specific and mass activities of different catalysts; reproduced with permission from ref.[66], Copyright 2016, American Association for the Advancement of Science; (C) ORR polarization curves of E-Pt NSs/C, A-Pt NSs/C, and commercial Pt/C; (D) mass activity and specific activity of different catalysts. Reproduced with permission from ref.[42], Copyright 2019, WILEY-VCH.

3.4 CO_2 Reduction Reaction(CO_2RR)

A large amount of CO_2 released by burning fossil fuels has caused increasingly serious environmental problems. Converting CO_2 into high value-added chemicals or liquid fuels is an ideal way to solve the problems of climate warming and energy crisis[148]. Therefore, CO_2 reduction technology has always been a research hotspot for researchers. Noble metal nanomaterials have shown wide application prospects in CO_2RR due to their low potential, high current density and

good selectivity[149].

Luo's group[150] discussed the effect of size and morphology of noble metal nanomaterials on electrocatalytic CO_2 reduction reaction performance. Through wet-chemical methods, they synthesized 2D triangular Ag nanoplates composed of two (111) planes and three (100) planes by reducing $AgNO_3$ aqueous solution in the presence of $NaBH_4$, H_2O_2 and trisodium citrate. As shown in Fig.14, compared with similarly sized Ag nanoparticles(SS-Ag-NPs) and bulk Ag, the as-prepared triangular silver nanoplates(Tri-Ag-NPs) exhibit enhanced current density and higher Faraday efficiency for CO formation at an extremely low overpotential of 0.746 V, which indicates that the CO_2RR catalytic efficiency is related to the shape of catalyst. Meanwhile, 2D Tri-Ag-NPs are the most active electrocatalyst in the formation of CO compared with other morphology Ag nanomaterials.

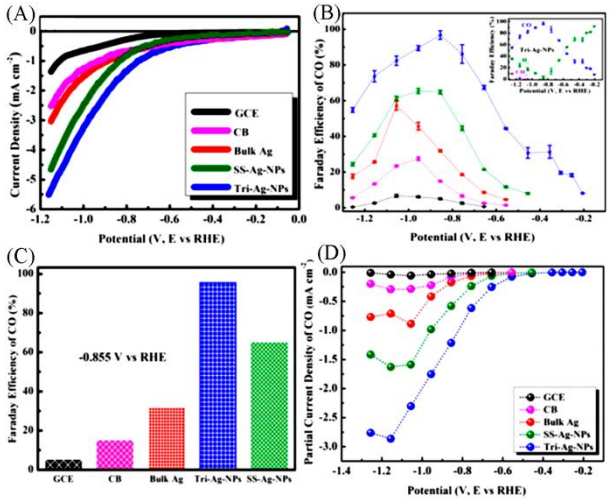

Fig.14 Electrochemical CO_2RR performance

(A) Cathodic LSV results of Tri-AgNPs; (B) FEs of CO under various applied potentials. Inset: the CO, CH_4 and H_2 overall FE for Tri-AgNPs; (C) CO FEs at a fixed potential of –0.855 V; (D) CO partial current density. Reproduced with permission from ref.[150], Copyright 2017, American Chemical Society.

4 Conclusions and Perspectives

2D NMNs exhibit excellent performance in the field of electrocatalysis due to their unique chemical, mechanical, and optoelectronic properties brought by special structure. In this review, we summarized the representative 2D NMNs and corresponding preparation strategies according to different metal elements, and the mechanisms behind these strategies are also discussed. It is strongly noted that some 2D NMNs reveal excellent performance in catalyzing reactions related to renewable energy like HER，OER，ORR and CO_2RR. It combines the merits of both noble metal and 2D nanostructures, while bridges the unique features between them. Firstly, the high specific surface area and abundantly exposed surface atoms of 2D NMNs are deemed to be responsible for their higher electrocatalytic activity compared with the 0-1 dimensional metal counterparts. Secondly, by means of fine regulating towards 2D NMNs(such as element doping and surface modification), the properties get obviously improved for electrocatalysis. Furthermore, the 2D noble metal-based nanomaterials can be used as a host substrate material to support atomically dispersed metals. Combining the concepts of size and alloying effect, the synergistic effects between noble metals substrate and the single-atom component can greatly boost the quality activity of the single atom alloy catalyst.

Although the great progress has been made in synthesis and applications of 2D NMNs, there are still lots of challenges existing in this field. Firstly, due to the complex growth mechanism and structure-property relationship of 2D materials, the thorough comprehension of their formation is still fuzzy despite the achieved multiple synthesis methods. In recent years, the rapid development of *in-situ* technology, such as *in-situ* transmission electron microscope, *in-situ* synchrotron radiation spectrum and *in-situ* Raman spectrum, provides a chance for deeper research on 2D NMNs formation mechanism. The combination of various *in-situ* technologies is required in this regard. Secondly, the wet-chemical method commonly always introduces surfactants, which can cause unwished activity degradation. Therefore, an effective surface-cleaning synthesis strategy is in sore need with simultaneous free of surfactants and stable 2D structure. Thirdly, from the view of practical application, the study of 2D NMNs remains at the stage in laboratory. Their yield and quality are far from the demand in industrialization and commercialization. More convenient and effective preparation methods are called to boost the scale application considering the high cost of noble metals. Fourth, metal nanomaterials with different crystal phases usually exhibit special performance due to changes in the atomic arrangement and electronic structure, and have potential in various applications. However, it is still a big challenge for the crystal phase engineering of 2D NMNs, and it was rarely reported of 2D NMNs with novel crystal phases. Generally, internal stress and surface stress play a crucial role in regulating the crystal phase of 2D NMNs. Researchers should pay attention to the preparation method of 2D NMNs to obtain a novel crystal phase(such as the amorphous phase) and the transformation between different phases, which will be a potential research direction. Last but not the least, regarding the physical and chemical properties of materials, single 2D NMNs is quite a limited system. Construction of appropriate heterostructure could promote their performance. As a result, exploitation of the composite structure of 2D NMNs as highly active substrate and low dimension materials(like 0D-2D and 1D-2D), and even with 3D structure, may become an interesting area for high performance catalysts.

In conclusion, there remains lots of space for research about synthesis and application of 2D NMNs, facing both opportunities and challenges. We believe that following the deepening of theoretical research and experiments, 2D NMNs ascend the heights by right of its unique properties and then wider applications.

References

[1] Tan C., Cao X., Wu X. J., He Q., Yang J., Zhang X., Chen J., Zhao W., Han S., Nam G. H., Sindoro M., Zhang H., *Chem. Rev.*, **2017**, *117*, 6225

[2] Nasilowski M., Mahler B., Lhuillier E., Ithurria S., Dubertret B.,

Chem. Rev., **2016**, *116*, 10934
[3] Jin H., Guo C., Liu X., Liu J., Vasileff A., Jiao Y., Zheng Y., Qiao S. Z., *Chem. Rev.*, **2018**, *118*, 6337
[4] Deng D., Novoselov K. S., Fu Q., Zheng N., Tian Z., Bao X., *Nat. Nanotechnol.*, **2016**, *11*, 218
[5] Xia Y., Yang X., *Accounts Chem. Res.*, **2017**, *50*, 450
[6] Luo Y., Liu Z., Wu G., Wang G., Chao T., Li H., Liu J., Hong X., *Chin. Chem. Lett.*, **2019**, *30*, 1093
[7] Ge Y., Shi Z., Tan C., Chen Y., Cheng H., He Q., Zhang H., *Chem.*, **2020**, *6*, 1237
[8] Novoselov K. S., Geim A. K., Morozov S. V., Jiang D., Zhang Y., Dubonos S. V., Grigorieva I. V., Firsov A. A., *Science*, **2004**, *306*, 666
[9] Nair R. R., Blake P., Grigorenko A. N., Novoselov K. S., Booth T. J., Stauber T., Peres N. M., Geim A. K., *Science*, **2008**, *320*, 1308
[10] Weng Q., Wang X., Wang X., Bando Y., Golberg D., *Chem. Soc. Rev.*, **2016**, *45*, 3989
[11] Zhang J., Chen Y., Wang X., *Energy Environ. Sci.*, **2015**, *8*, 3092
[12] Hong X., Tan C., Chen J., Xu Z., Zhang H., *Nano Res.*, **2014**, *8*, 40
[13] Peng Y., Li Y., Ban Y., Jin H., Jiao W., Liu X., Yang W., *Science*, **2014**, *346*, 1356
[14] Peng Y., Huang Y., Zhu Y., Chen B., Wang L., Lai Z., Zhang Z., Zhao M., Tan C., Yang N., Shao F., Han Y., Zhang H., *J. Am. Chem. Soc.*, **2017**, *139*, 8698
[15] Wu G., Chen W., Zheng X., He D., Luo Y., Wang X., Yang J., Wu Y., Yan W., Zhuang Z., Hong X., Li Y., *Nano Energy*, **2017**, *38*, 167
[16] Ling T., Wang J. J., Zhang H., Song S. T., Zhou Y. Z., Zhao J., Du X. W., *Adv. Mater.*, **2015**, *27*, 5396
[17] Ma Y., Li B., Yang S., *Mater. Chem. Front.*, **2018**, *2*, 456
[18] Cheng H., Yang N., Lu Q., Zhang Z., Zhang H., *Adv. Mater.*, **2018**, *30*, e1707189
[19] Zeb Gul Sial M. A., Ud Din M. A., Wang X., *Chem. Soc. Rev.*, **2018**, *47*, 6175
[20] Zhang B., Zheng X., Voznyy O., Comin R., Bajdich M., Garcia-Melchor M., Han L., Xu J., Liu M., Zheng L., Arquer F. P. G., Dinh C. T., Fan F., Yuan M., Yassitepe E., Chen N., Regier T., Liu P., Li Y., Luna P. D., Janmohamed A., Xin H. L., Yang H., Vojvodic A., Sargent E. H., *Science*, **2016**, *352*, 333
[21] Jiao Y., Zheng Y., Jaroniec M., Qiao S. Z., *Chem. Soc. Rev.*, **2015**, *44*, 2060
[22] Debe M. K., *Nature*, **2012**, *486*, 43
[23] Chao T., Hu Y., Hong X., Li Y., *ChemElectroChem*, **2019**, *6*, 289
[24] Seh Z. W., Kibsgaard J., Dickens C. F., Chorkendorff I., Norskov J. K., Jaramillo T. F., *Science*, **2017**, *355*, eaad4998
[25] Shao M., Chang Q., Dodelet J. P., Chenitz R., *Chem. Rev.*, **2016**, *116*, 3594
[26] Strmcnik D., Uchimura M., Wang C., Subbaraman R., Danilovic N., van der Vliet D., Paulikas A. P., Stamenkovic V. R., Markovic N. M., *Nat. Chem.*, **2013**, *5*, 300
[27] Suen N. T., Hung S. F., Quan Q., Zhang N., Xu Y. J., Chen H. M., *Chem. Soc. Rev.*, **2017**, *46*, 337
[28] Zhu D. D., Liu J. L., Qiao S. Z., *Adv. Mater.*, **2016**, *28*, 3423
[29] Kulkarni A., Siahrostami S., Patel A., Norskov J. K., *Chem. Rev.*, **2018**, *118*, 2302
[30] McCrory C. C., Jung S., Ferrer I. M., Chatman S. M., Peters J. C., Jaramillo T. F., *J. Am. Chem. Soc.*, **2015**, *137*, 4347
[31] Liu H. L., Nosheen F., Wang X., *Chem. Soc. Rev.*, **2015**, *44*, 3056
[32] Liu S., Tian N., Xie A. Y., Du J. H., Xiao J., Liu L., Sun H. Y., Cheng Z. Y., Zhou Z. Y., Sun S. G., *J. Am. Chem. Soc.*, **2016**, *138*, 5753
[33] Hong X., Wang D., Cai S., Rong H., Li Y., *J. Am. Chem. Soc.*, **2012**, *134*, 18165
[34] Ge J., Li Z., Hong X., Li Y., *Chem. Eur. J.*, **2019**, *25*, 5113
[35] Zou X., Zhang Y., *Chem. Soc. Rev.*, **2015**, *44*, 5148
[36] Hunter B. M., Gray H. B., Muller A. M., *Chem. Rev.*, **2016**, *116*, 14120
[37] Yang M. Q., Wang J., Wu H., Ho G. W., *Small*, **2018**, *14*, e1703323
[38] Zhu C., Du D., Eychmuller A., Lin Y., *Chem. Rev.*, **2015**, *115*, 8896
[39] Ren X., Lv Q., Liu L., Liu B., Wang Y., Liu A., Wu G., *Sust. Energy Fuels*, **2020**, *4*, 15
[40] Wang Y., Mao J., Meng X., Yu L., Deng D., Bao X., *Chem. Rev.*, **2019**, *119*, 1806
[41] An B., Li M., Wang J., Li C., *Front. Chem. Sci. Eng.*, **2016**, *10*, 360
[42] Feng Y., Huang B., Yang C., Shao Q., Huang X., *Adv. Funct. Mater.*, **2019**, *29*, 1904429
[43] Zhang H., *ACS Nano*, **2015**, *9*, 9451
[44] Chia X., Pumera M., *Nat. Catal.*, **2018**, *1*, 909
[45] Dou Y., Zhang L., Xu X., Sun Z., Liao T., Dou S. X., *Chem. Soc. Rev.*, **2017**, *46*, 7338
[46] Xia Y., Xiong Y., Lim B., Skrabalak S. E., *Angew. Chem. Int. Ed.*, **2009**, *48*, 60
[47] Luo M., Sun Y., Wang L., Guo S., *Adv. Energy Mater.*, **2017**, *7*, 1602073
[48] Liz-Marzan L. M., Grzelczak M., *Science*, **2017**, *356*, 1120
[49] Xie S., Liu X. Y., Xia Y., *Nano Res.*, **2015**, *8*, 82
[50] Chen Y., Fan Z., Zhang Z., Niu W., Li C., Yang N., Chen B., Zhang H., *Chem. Rev.*, **2018**, *118*, 6409
[51] Fan Z., Zhang H., *Accounts Chem. Res.*, **2016**, *49*, 2841
[52] Yi M., Shen Z., *J. Mater. Chem. A*, **2015**, *3*, 11700
[53] Lizmarzan L. M., Grzelczak M., *Science*, **2017**, *356*, 1120
[54] Wang F., Wang Z., Shifa T. A., Wen Y., Wang F., Zhan X., Wang Q., Xu K., Huang Y., Yin L., Jiang C., He J., *Adv. Funct. Mater.*, **2017**, *27*, 1603254
[55] Lee J., Yang J., Kwon S. G., Hyeon T., *Nat. Rev. Mater.*, **2016**, *1*, 16034
[56] Gilroy K. D., Ruditskiy A., Peng H. C., Qin D., Xia Y., *Chem. Rev.*, **2016**, *116*, 10414
[57] O'Brien M. N., Jones M. R., Kohlstedt K. L., Schatz G. C., Mirkin C. A., *Nano Lett.*, **2015**, *15*, 1012
[58] Funatsu A., Tateishi H., Hatakeyama K., Fukunaga Y., Taniguchi T., Koinuma M., Matsuura H., Matsumoto Y., *Chem. Commun.*, **2014**, *50*, 8503
[59] Xu D., Lv H., Jin H., Liu Y., Ma Y., Han M., Bao J., Liu B., *J. Phys. Chem. Lett.*, **2019**, *10*, 663
[60] Xie B., Zhang Y., Du N., Li H., Hou W., Zhang R., *Chem. Commun.*, **2016**, *52*, 13815
[61] Liu H., Zhong P., Liu K., Han L., Zheng H., Yin Y., Gao C., *Chem. Sci.*, **2018**, *9*, 398
[62] Chhetri M., Rana M., Loukya B., Patil P. K., Datta R., Gautam U. K., *Adv. Mater.*, **2015**, *27*, 4430
[63] Huang X., Zeng Z., Bao S., Wang M., Qi X., Fan Z., Zhang H., *Nat. Commun.*, **2013**, *4*, 1444
[64] Dai L., Zhao Y., Qin Q., Zhao X., Xu C., Zheng N., *ChemNanoMat*, **2016**, *2*, 776
[65] Qin Y., Luo M., Sun Y., Li C., Huang B., Yang Y., Li Y., Wang L., Guo S., *ACS Catal.*, **2018**, *8*, 5581
[66] Bu L., Zhang N., Guo S., Zhang X., Li J., Yao J., Wu T., Lu G., Ma J.,

Su D., Huang X., *Science*, **2016**, *354*, 1410
[67] Liao H., Zhu J., Hou Y., *Nanoscale*, **2014**, *6*, 1049
[68] Saleem F., Zhang Z., Xu B., Xu X., He P., Wang X., *J. Am. Chem. Soc.*, **2013**, *135*, 18304
[69] Saleem F., Zhang Z., Cui X., Gong Y., Chen B., Lai Z., Yun Q., Gu L., Zhang H., *J. Am. Chem. Soc.*, **2019**, *141*, 14496
[70] Zhang H., Jin M., Xiong Y., Lim B., Xia Y., *Accounts Chem. Res.*, **2013**, *46*, 1783
[71] Lim B., Jiang M., Tao J., Camargo P. H. C., Zhu Y., Xia Y., *Adv. Funct. Mater.*, **2009**, *19*, 189
[72] Luo M., Zhao Z., Zhang Y., Sun Y., Xing Y., Lv F., Yang Y., Zhang X., Hwang S., Qin Y., Ma J. Y., Lin F., Su D., Lu G., Guo S., *Nature*, **2019**, *574*, 81
[73] Surnev S., Sock M., Ramsey M. G., Netzer F. P., Wiklund M., Borg M., Andersen J. N., *Surf. Sci.*, **2000**, *470*, 171
[74] Siril P. F., Ramos L., Beaunier P., Archirel P., Etcheberry A., Remita H., *Chem. Mater.*, **2009**, *21*, 5170
[75] Huang X., Tang S., Mu X., Dai Y., Chen G., Zhou Z., Ruan F., Yang Z., Zheng N., *Nat. Nanotechnol.*, **2010**, *6*, 28
[76] Li H., Chen G., Yang H., Wang X., Liang J., Liu P., Chen M., Zheng N., *Angew. Chem. Int. Ed.*, **2013**, *52*, 8368
[77] Yin X., Liu X., Pan Y. T., Walsh K. A., Yang H., *Nano Lett.*, **2014**, *14*, 7188
[78] Hong J. W., Kim Y., Wi D. H., Lee S., Lee S. U., Lee Y. W., Choi S. I., Han S. W., *Angew. Chem. Int. Ed.*, **2016**, *55*, 2753
[79] Puntes V. F., Zanchet D., Erdonmez C. K., Alivisatos A. P., *J. Am. Chem. Soc.*, **2002**, *124*, 12874
[80] Yang N., Zhang Z., Chen B., Huang Y., Chen J., Lai Z., Chen Y., Sindoro M., Wang A. L., Cheng H., Fan Z., Liu X., Li B., Zong Y., Gu L., Zhang H., *Adv. Mater.*, **2017**, *29*, 1700769.1
[81] Wang Y., Peng H. C., Liu J., Huang C. Z., Xia Y., *Nano Lett.*, **2015**, *15*, 1445
[82] Huang W., Kang X., Xu C., Zhou J., Deng J., Li Y., Cheng S., *Adv. Mater.*, **2018**, *30*, 1706962.1
[83] Qiu X., Zhang H., Wu P., Zhang F., Wei S., Sun D., Xu L., Tang Y., *Adv. Funct. Mater.*, **2017**, *27*, 1603852.1
[84] Liu J., Ma Q., Huang Z., Liu G., Zhang H., *Adv. Mater.*, **2019**, *31*, e1800696
[85] Jiang Y., Yan Y., Chen W., Khan Y., Wu J., Zhang H., Yang D., *Chem. Commun.*, **2016**, *52*, 14204
[86] He C., Tao J., Shen P. K., *ACS Catal.*, **2018**, *8*, 910
[87] Hu Y., Luo X., Wu G., Chao T., Li Z., Qu Y., Li H., Wu Y., Jiang B., Hong X., *ACS Appl. Mater. Interfaces*, **2019**, *11*, 42298
[88] Ge J., He D., Chen W., Ju H., Zhang H., Chao T., Wang X., You R., Lin Y., Wang Y., Zhu J., Li H., Xiao B., Huang W., Wu Y., Hong X., Li Y., *J. Am. Chem. Soc.*, **2016**, *138*, 13850
[89] Ge J., Wei P., Wu G., Liu Y., Yuan T., Li Z., Qu Y., Wu Y., Li H., Zhuang Z., Hong X., Li Y., *Angew. Chem. Int. Ed.*, **2018**, *57*, 3435
[90] Li N., Zhao P., Astruc D., *Angew. Chem. Int. Ed.*, **2014**, *53*, 1756
[91] Fan Z., Huang X., Chen Y., Huang W., Zhang H., *Nat. Protoc.*, **2017**, *12*, 2367
[92] Chen C. C., Hsu C. H., Kuo P. L., *Langmuir*, **2007**, *23*, 6801
[93] Jang M. H., Kim J. K., Tak H., Yoo H., *J. Mater. Chem.*, **2011**, *21*, 17606
[94] Hong X., Tan C. L., Liu J. Q., Yang J., Wu X. J., Fan Z. X., Luo Z. M., Chen J. Z., Zhang X., Chen B., Zhang H., *J. Am. Chem. Soc.*, **2015**, *137*, 1444
[95] Tsuji M., Gomi S., Maeda Y., Matsunaga M., Hikino S., Uto K., Tsuji T., Kawazumi H., *Langmuir*, **2012**, *28*, 8845
[96] Lohse S. E., Burrows N. D., Scarabelli L., Liz-Marzán L. M., Murphy C. J., *Chem. Mat.*, **2013**, *26*, 34
[97] Hwang S. Y., Zhang M., Zhang C., Ma B., Zheng J., Peng Z., *Chem. Commun.*, **2014**, *50*, 14013
[98] Chen M., Wu B., Yang J., Zheng N., *Adv. Mater.*, **2012**, *24*, 862
[99] Long R., Zhou S., Wiley B. J., Xiong Y., *Chem. Soc. Rev.*, **2014**, *43*, 6288
[100] Chen L., Ji F., Xu Y., He L., Mi Y., Bao F., Sun B., Zhang X., Zhang Q., *Nano Lett.*, **2014**, *14*, 7201
[101] Huang X., Qi X., Huang Y., Li S., Xue C., Gan C. L., Boey F., Zhang H., *ACS Nano*, **2010**, *4*, 6196
[102] Shaik F., Zhang W., Niu W., *J. Phys. Chem. C*, **2017**, *121*, 9572
[103] Brus L., *Nat. Mater.*, **2016**, *15*, 824
[104] DuChene J. S., Niu W., Abendroth J. M., Sun Q., Zhao W., Huo F., Wei W. D., *Chem. Mater.*, **2012**, *25*, 1392
[105] Zhai Y., DuChene J. S., Wang Y. C., Qiu J., Johnston-Peck A. C., You B., Guo W., DiCiaccio B., Qian K., Zhao E. W., Ooi F., Hu D., Su D., Stach E. A., Zhu Z., Wei W. D., *Nat. Mater.*, **2016**, *15*, 889
[106] Niu J., Wang D., Qin H., Xiong X., Tan P., Li Y., Liu R., Lu X., Wu J., Zhang T., Ni W., Jin J., *Nat. Commun.*, **2014**, *5*, 3313
[107] Zhou M., Lin M., Chen L., Wang Y., Guo X., Peng L., Guo X., Ding W., *Chem. Commun.*, **2015**, *51*, 5116
[108] Wang L., Zhu Y., Wang J. Q., Liu F., Huang J., Meng X., Basset J. M., Han Y., Xiao F. S., *Nat. Commun.*, **2015**, *6*, 6957
[109] Huang X., Li S., Huang Y., Wu S., Zhou X., Li S., Gan C. L., Boey F., Mirkin C. A., Zhang H., *Nat. Commun.*, **2011**, *2*, 292
[110] Fan Z., Bosman M., Huang X., Huang D., Yu Y., Ong K. P., Akimov Y. A., Wu L., Li B., Wu J., Huang Y., Liu Q., Png C. E., Gan C. L., Yang P., Zhang H., *Nat. Commun.*, **2015**, *6*, 7684
[111] Fan Z., Zhu Y., Huang X., Han Y., Zhang H., *Angew. Chem. Int. Ed.*, **2015**, *54*, 5672
[112] Fan Z., Luo Z., Huang X., Li B., Chen Y., Wang J., Hu Y., Zhang H., *J. Am. Chem. Soc.*, **2016**, *138*, 1414
[113] Fan Z., Luo Z., Chen Y., Wang J., Li B., Zong Y., Zhang H., *Small*, **2016**, *12*, 3908
[114] Millstone J. E., Hurst S. J., Metraux G. S., Cutler J. I., Mirkin C. A., *Small*, **2009**, *5*, 646
[115] Jin R., Cao Y., Mirkin C. A., Kelly K. L., Schatz G. C., Zheng J. G., *Science*, **2001**, *294*, 1901
[116] Jin R., Cao Y. C., Hao E., Metraux G. S., Schatz G. C., Mirkin C. A., *Nature*, **2003**, *425*, 487
[117] Xue C., Millstone J. E., Li S., Mirkin C. A., *Angew. Chem. Int. Ed.*, **2007**, *46*, 8436
[118] Kim M. H., Kwak S. K., Im S. H., Lee J. B., Choi K. Y., Byun D. J., *J. Mater. Chem. C*, **2014**, *2*, 6165
[119] Zhang Q., Li N., Goebl J., Lu Z., Yin Y., *J. Am. Chem. Soc.*, **2011**, *133*, 18931
[120] Zeng J., Xia X., Rycenga M., Henneghan P., Li Q., Xia Y., *Angew. Chem. Int. Ed.*, **2011**, *50*, 244
[121] Liu H., Tang H., Fang M., Si W., Zhang Q., Huang Z., Gu L., Pan W., Yao J., Nan C., Wu H., *Adv. Mater.*, **2016**, *28*, 8170
[122] Chiou W. H., Wang Y. W., Kao C. L., Chen P. C., Wu C. C., *Organometallics*, **2014**, *33*, 4240
[123] Zhao L., Xu C., Su H., Liang J., Lin S., Gu L., Wang X., Chen M., Zheng N., *Adv. Sci.*, **2015**, *2*, 1500100
[124] Hou C., Zhu J., Liu C., Wang X., Kuang Q., Zheng L., *CrystEngComm*, **2013**, *15*, 6127

[125] Duan H., Yan N., Yu R., Chang C. R., Zhou G., Hu H. S., Rong H., Niu Z., Mao J., Asakura H., Tanaka T., Dyson P. J., Li J., Li Y., *Nat. Commun.*, **2014**, *5*, 3093

[126] Pi Y., Zhang N., Guo S., Guo J., Huang X., *Nano Lett.*, **2016**, *16*, 4424

[127] Jiang B., Guo Y., Kim J., Whitten A. E., Wood K., Kani K., Rowan A. E., Henzie J., Yamauchi Y., *J. Am. Chem. Soc.*, **2018**, *140*, 12434

[128] Yin A. X., Liu W. C., Ke J., Zhu W., Gu J., Zhang Y. W., Yan C. H., *J. Am. Chem. Soc.*, **2012**, *134*, 20479

[129] Kong X., Xu K., Zhang C., Dai J., Norooz Oliaee S., Li L., Zeng X., Wu C., Peng Z., *ACS Catal.*, **2016**, *6*, 1487

[130] Yao Q., Huang B., Zhang N., Sun M., Shao Q., Huang X., *Angew. Chem. Int. Ed.*, **2019**, *58*, 13983

[131] Mao J., He C. T., Pei J., Chen W., He D., He Y., Zhuang Z., Chen C., Peng Q., Wang D., Li Y., *Nat. Commun.*, **2018**, *9*, 4958

[132] Wu G., Zheng X., Cui P., Jiang H., Wang X., Qu Y., Chen W., Lin Y., Li H., Han X., Hu Y., Liu P., Zhang Q., Ge J., Yao Y., Sun R., Wu Y., Gu L., Hong X., Li Y., *Nat. Commun.*, **2019**, *10*, 4855

[133] Chhowalla M., Shin H. S., Eda G., Li L. J., Loh K. P., Zhang H., *Nat. Chem.*, **2013**, *5*, 263

[134] Wang Q., O'Hare D., *Chem. Rev.*, **2012**, *112*, 4124

[135] Naguib M., Mochalin V. N., Barsoum M. W., Gogotsi Y., *Adv. Mater.*, **2014**, *26*, 992

[136] Wang G., Tao J., Zhang Y., Wang S., Yan X., Liu C., Hu F., He Z., Zuo Z., Yang X., *ACS Appl. Mater. Interfaces*, **2018**, *10*, 25409

[137] Lu X., Xie S., Yang H., Tong Y., Ji H., *Chem. Soc. Rev.*, **2014**, *43*, 7581

[138] Luo Y., Luo X., Wu G., Li Z., Wang G., Jiang B., Hu Y., Chao T., Ju H., Zhu J., Zhuang Z., Wu Y., Hong X., Li Y., *ACS Appl. Mater. Interfaces*, **2018**, *10*, 34147

[139] Higgins D., Zamani P., Yu A., Chen Z., *Energy Environ. Sci.*, **2016**, *9*, 357

[140] Yin H., Zhao S., Zhao K., Muqsit A., Tang H., Chang L., Zhao H., Gao Y., Tang Z., *Nat. Commun.*, **2015**, *6*, 6430

[141] Yao T., An X., Han H., Chen J. Q., Li C., *Adv. Energy Mater.*, **2018**, *8*, 1800210

[142] Yao Y., Gu X. K., He D., Li Z., Liu W., Xu Q., Yao T., Lin Y., Wang H. J., Zhao C., Wang X., Yin P., Li H., Hong X., Wei S., Li W. X., Li Y., Wu Y., *J. Am. Chem. Soc.*, **2019**, *141*, 19964

[143] Chao T., Luo X., Chen W., Jiang B., Ge J., Lin Y., Wu G., Wang X., Hu Y., Zhuang Z., Wu Y., Hong X., Li Y., *Angew. Chem. Int. Ed.*, **2017**, *56*, 16047

[144] Man I. C., Su H. Y., Calle-Vallejo F., Hansen H. A., Martínez J. I., Inoglu N. G., Kitchin J., Jaramillo T. F., Nørskov J. K., Rossmeisl J., *ChemCatChem*, **2011**, *3*, 1159

[145] Chu S., Cui Y., Liu N., *Nat. Mater.*, **2016**, *16*, 16

[146] Cano Z. P., Banham D., Ye S., Hintennach A., Lu J., Fowler M., Chen Z., *Nat. Energy*, **2018**, *3*, 279

[147] Winther-Jensen B., Winther-Jensen O., Forsyth M., Macfarlane D. R., *Science*, **2008**, *321*, 671

[148] Buitenwerf R., Rose L., Higgins S. I., *Nat. Clim. Change.*, **2015**, *5*, 364

[149] Rogers C., Perkins W. S., Veber G., Williams T. E., Cloke R. R., Fischer F. R., *J. Am. Chem. Soc.*, **2017**, *139*, 4052

[150] Liu S., Tao H., Zeng L., Liu Q., Xu Z., Liu Q., Luo J. L., *J. Am. Chem. Soc.*, **2017**, *139*, 2160